Virologic and Immunologic Events in Hilar Lymph Nodes During Simian Immunodeficiency Virus Infection

Development of Polarized Inflammation

Beth A. Fallert, BS, Sandra Poveda, BS, Todd M Schaefer, PhD, Melanie E. Pfeifer, BS, Sonali K. Sanghavi, MD, PhD, Simon C. Watkins, PhD, Michael A. Murphey-Corb, PhD, Patrick M. Tarwater, PhD, Denise E. Kirschner, PhD, and Todd A. Reinhart, ScD

Summary: Lymphoid tissues are sites of soluble and cell-associated antigen sampling of peripheral tissues, and they are key compartments for the generation of cellular and humoral immune responses. Hilar lymph nodes (HiLNs), which drain the lungs, were examined to understand the effects of simian immunodeficiency virus (SIV) infection on this compartment of the immune system. Histologic and messenger RNA (mRNA) expression profiling approaches were used to determine the numbers, types, and distributions of SIV viral RNA^+ cells and to identify differentially expressed genes in HiLNs during SIV infection. SIV RNA^+ cells were found to be primarily $CD68^-$ and localized to paracortical and medullary regions early in infection, whereas they resided mainly in paracortex during AIDS. As SIV infection progressed, CXCL9, CXCL10, interferon-γ, and Toll-like receptor 3 levels all increased. In contrast, CCL19 increased early in infection but decreased during AIDS, whereas CCL21 decreased progressively throughout infection. Finally, local levels of cellular activation were increased throughout infection. Taken together, these findings indicate that SIV infection leads to an inflammatory environment in lung-draining lymph nodes that is characterized by type 1 cytokines and chemokines and likely has an impact on the nature and strength of immune responses to pulmonary pathogens.

Key Words: immunohistochemistry, in situ hybridization, lung, lymph node, simian immunodeficiency virus

(*J Acquir Immune Defic Syndr* 2008;47:16–26)

During HIV-1 infection and AIDS, opportunistic infections frequently develop in the lungs,[1,2] such as those by *Pneumocystis carinii*[3] and *Mycobacterium tuberculosis*.[4] The propensity to develop *P. carinii* pneumonia is a hallmark of HIV-1 and simian immunodeficiency virus (SIV) infection[3,5] and underscores the role of this large interface between the host and the environment in the disease process. In addition, infection by opportunistic pathogens and HIV-1 is interrelated. For example, *M. tuberculosis* infection seems to accelerate HIV-1 disease progression,[6] and HIV-1 infection increases the incidence and severity of tuberculosis in coinfected individuals and increases reactivation rates from latent tuberculosis.[4]

The hilar lymph nodes (HiLNs) drain the lungs, and examination of the virologic and immunologic activities in this lymphoid compartment could provide insight into mechanisms leading to pulmonary complications during HIV-1 infection. Fluids and cells draining from the lungs could contribute to shaping the environments in HiLNs. In turn, events in HiLNs control the potency and nature of lung-homing effector T-cell responses. Despite these intercompartmental relations, the extent of viral replication and sets of viral variants in lymph nodes (LNs) can be different from the extent reflected in lung tissues.[6–8] Therefore, to understand better the events that contribute to the shaping of immune responses to pulmonary pathogens, it is necessary to study the lymphoid tissues that drain the lungs.

Lymphoid tissues serve as a major reservoir and site of viral replication during HIV-1[9,10] and SIV[11,12] infections. Lymphoid tissues have been studied to determine the effects of HIV-1 or SIV infection, but only limited analyses have been performed specifically of pulmonary draining LNs. Toward this end, we examined HiLNs to obtain a better understanding of the effects of HIV-1 infection on this immune environment. Using the SIV/macaque model, we examined the effects of SIV infection on the local immune environment by identifying differentially expressed messenger RNAs (mRNAs) and measuring changes in cell populations and gene expression levels directly in tissues. These studies revealed an inflammatory response that likely fuels ongoing viral replication and contributes to loss of overall immune function.

MATERIALS AND METHODS

Animals and Tissue Processing

All animal studies were performed under the approval and guidance of the University of Pittsburgh Institutional Animal Care and Use Committee. The 27 adult rhesus macaques (*Macaca mulatta*) and 5 cynomolgus macaques

Received for publication June 29, 2007; accepted October 2, 2007.
From the Department of Infectious Diseases and Microbiology, Graduate School of Public Health, University of Pittsburgh, Pittsburgh, PA.
Supported by grants from the National Institutes of Health (grants HL62056 and AI060422 to T. A. Reinhart and grant HL072682 to D. E. Kirschner) and from the Office of Research of The University of Pittsburgh School of Medicine.
Correspondence to: Todd A. Reinhart, ScD, Department of Infectious Diseases and Microbiology, Graduate School of Public Health, University of Pittsburgh, 130 DeSoto Street, Pittsburgh, PA 15261 (e-mail: reinhar@pitt.edu).

(*Macaca fascicularis*) were negative for SIV; simian retrovirus (type D); and simian T-lymphotrophic viruses -1, -2, and -3. Twenty-three macaques were inoculated intravenously and 3 were inoculated intratracheally with the pathogenic SIV/DeltaB670 isolate.[13] Twelve rhesus macaques were killed 2 weeks after injection, 4 at 8 weeks after injection, and 6 on development of AIDS. Ten uninfected macaques were available for inclusion as controls, 5 of which were rhesus macaques and 5 of which were cynomolgus macaques. Uninfected cynomolgus macaques were included in this study because at the onset, snap-frozen HiLNs were not available from rhesus macaques. Tissues from 3 uninfected rhesus macaques ultimately became available. The uninfected cynomolgus macaque HiLN samples served as the uninfected controls in the microarray hybridization studies, whereas they were included in parallel with rhesus macaque samples in the real-time reverse transcriptase polymerase chain reaction (RT-PCR) and microscope slide–based analyses.

At necropsy, transcardial perfusion was performed with 0.9% saline to remove contaminating blood cells from tissues. Tissue specimens were fixed by immersion in fresh 4% paraformaldehyde (PF)/phosphate-buffered saline (PBS) and processed as described elsewhere.[14]

In Situ Hybridization and Immunostaining

In situ hybridization (ISH) with ^{35}S-labeled riboprobes and immunohistochemistry (IHC) were performed as described elsewhere.[14,15] Autoradiographic exposure times were 7 days. Antibodies used for IHC were specific for Ki67 (Novocastra, Newcastle, UK; clone MM1, 1:100), CD20 (Dako; clone L26, 1:100), CD3 (Novocastra; clones CD3 to CD12, 1:100), fascin/p55 (Dako; clone 55K-2, 1:100), CD68 (Dako, Glostrup, Denmark; clone KP1, 1:50), and human leukocyte antigen D-related (HLA-DR) (Dako; clone TAL.1B5, 1:25).

Two-color fluorescence immunostaining of tissue sections was performed by incubating pretreated[14,15] tissue sections with primary antibodies, washing in PBS, and incubation with fluorescein- or biotin-SP–conjugated secondary antibody (Jackson ImmunoResearch Laboratories, West Grove, PA). After washing in PBS, sections were then incubated with AlexaFluor-488–conjugated antifluorescein antibody or AlexFluor-647–conjugated streptavidin (Molecular Probes, Carlsbad, CA). Sections were treated with Autofluorescence Eliminator (Chemicon, Temecula, CA) and mounted with Prolong Gold Antifade containing 4′,6-diamidino-2-phenylindole (DAPI) (Molecular Probes). When primary antibodies were from the same species, staining for individual antigens was performed sequentially with brief fixation in 4% PF/PBS performed between staining steps. Laser scanning confocal microscopy was performed with an Olympus (Center Valley, PA) Fluoview 500 microscope through a ×40 objective. Images were captured in the fluorescein isothiocyanate (FITC) and Cy5 channels and under differential interference contrast (DIC).

Real-Time RT-PCR

Real-time RT-PCR was performed on total RNA that was extracted from snap-frozen tissues as previously described[16] using Taqman chemistry. Primers and probes were previously described for interferon-γ (IFNγ)[15] and toll-like receptor 3 (TLR3),[16] and TaqMan human gene expression assays (Applied Biosystems, Foster City, CA) were used for CXCL9, CCL19, CCL21, and β-glucuronidase (β-GUS). Primers were designed for CXCL10 using the Primer Express software package (Applied Biosystems) and consisted of the sequences F1: GTCCACATGTTGAGATCATTGC and R1: TCTTGATGGCCTTAGATTCTGGAT and the probe sequence 6FAM- ACAATGAAAAAGAAGGGTGAGAAGAG GTGTCTG-TAMRA. mRNA expression levels were calculated with the comparative cycle threshold (C_T) method,[15–17] using an uninfected macaque RNA sample as the calibrator and β-GUS as the endogenous control mRNA. Real-time RT-PCR measurement of tissue-associated SIV viral loads was performed as described elsewhere[16] and presented as SIV RNA copies/μg of total RNA. Quantitation of virion-associated RNA in plasma was performed by real-time RT-PCR with an external standard curve.[18]

DNA Array Hybridization and Analysis

An immunologically focused macaque complementary DNA (cDNA) microarray was fabricated as described.[19] Total RNAs from HiLNs were labeled, reverse transcribed, and then hybridized to the array, which was stringently washed and then scanned and analyzed as described.[19]

Image Capture and Analysis

SIV viral ($vRNA^+$) cells were counted in 5 random microscopic fields viewed through a ×60 Plan Apochromat objective in follicular, cortical, and medullary regions of HiLN tissue sections. The mean values were calculated and normalized to cells/mm^2.

ISH signals for CXCL9 and CCL19 mRNAs were scored on a − to +++ scale, in which − represented a complete absence of signal and + represented low, ++ represented medium, and +++ represented high level of expression, giving consideration to the numbers of positive cells and signals per cell.

Quantitation of IHC signals was performed using a SPOT charged-couple device (CCD) (Diagnostic Instruments, Sterling Heights, MD) camera mounted on a Nikon (Melville, NY) E600 microscope fitted with a ×60 Plan Apochromat objective. Images were captured, and the surface areas covered by opaque 3,3′-diaminobenzidine (DAB) IHC product were measured using the threshold and measure tools of the MetaVue software package (Universal Imaging, West Chester, PA).

Analysis of the relations between CXCL9 and CCL19 ISH signals and CD68 and fascin/p55 IHC signals was performed on tissues simultaneously stained for antigen and hybridized for cellular RNAs. Regions of tissue sections were assigned a histologic score that spanned from 0 to 4 based on approximation of the percentage of RNA signal attributable to cells expressing the specific cell-type antigen, such that a score of 0 represented no attributable signal and scores of 1, 2, 3, and 4 represented approximate attributable signals of 1% to 25%, 26% to 50%, 51% to 75%, and 76% to 100%, respectively.

Fluorescently stained tissue sections were visually inspected and assigned a score for $Ki67^+$ cells that were also positive for a specific cell type marker (CD68, CD3, CD20, or p55) or CXCR3. A score was assigned based on evaluation of 3 random fields from each tissue.

Statistical Analyses

Each variable was described using the mean and standard deviation and medians with range and interquartile range. For comparisons between 2 groups, the Mann-Whitney comparison of 2 distributions was used. In addition, Pearson correlation coefficients and associated *P* values were calculated to estimate the association between 2 variables. *P* values of ≤ 0.05 were considered to be significant.

RESULTS

Virologic Events in HiLNs After SIV Infection

To understand better the virologic events occurring in lung-draining LNs during SIV infection, we examined this tissue from 22 rhesus macaques infected with the pathogenic SIV/DeltaB670 isolate, relative to uninfected controls (Table 1). Infected macaques were killed at 2 weeks after infection (acute), 8 weeks after infection (clinically latent), or on development of AIDS. To measure the local SIV burdens in HiLNs, we performed SIV-specific ISH (Fig. 1A–D) and real-time RT-PCR. Both approaches revealed higher levels of SIV infection during acute infection and clinical latency as compared with AIDS, with the exception of 3 macaques (see Table 1). There was a strong positive correlation between plasma viral loads and HiLN tissue viral loads in the follicular, paracortical, and medullary regions of HiLNs (r = 0.71 to 0.86, P values all <0.01). Interestingly, during the first 8 weeks after infection, the paracortex had the largest proportion of the infected cells in 10 of 13 animals, whereas

TABLE 1. Animals and Clinicovirologic States

Animal Number	Disease State	Species	Infection Route	Infection Duration (wk)	Plasma Viral Load*	SIV-Positive Cells/mm²†			
						Follicle	Paracortex	Medulla	SIV Copies/μg‡
M5600§	Uninfected	*M. mulatta*	N/A	N/A	ND	0	0	0	ND
M6600§	Uninfected	*M. mulatta*	N/A	N/A	ND	0	0	0	ND
R201	Uninfected	*M. mulatta*	N/A	N/A	ND	ND	ND	ND	ND
R205	Uninfected	*M. mulatta*	N/A	N/A	ND	ND	ND	ND	ND
R206	Uninfected	*M. mulatta*	N/A	N/A	ND	ND	ND	ND	ND
M5299§	Acute	*M. mulatta*	IV	2	10,000,000	56	118	71	ND
M5499§	Acute	*M. mulatta*	IV	2	6,500,000‖	99	148	95	ND
M5699§	Acute	*M. mulatta*	IV	2	63,000,000	28	82	ND	25,839
M5899§	Acute	*M. mulatta*	IV	2	14,000,000‖	0	10	3	ND
M0999§	Acute	*M. mulatta*	IV	2	29,000,000	24	24	24	ND
M5500	Acute	*M. mulatta*	IV	2	120,000,000	14	45	16	7115
M6400	Acute	*M. mulatta*	IV	2	2750	0	0	0	ND
M6800	Acute	*M. mulatta*	IV	2	140,000,000	33	62	12	ND
M12000	Acute	*M. mulatta*	IV	2	1,200,000,000	110	583	102	119,098
M13200	Acute	*M. mulatta*	IT	2	1,000,000,000	62	64	88	18,211
M13300	Acute	*M. mulatta*	IT	2	6,350,000	31	146	38	12,138
M13400	Acute	*M. mulatta*	IT	2	10,000	0	0	0	0
M5800	Clinically latent	*M. mulatta*	IV	8	55,000,000	40	108	43	82,128
M6100	Clinically latent	*M. mulatta*	IV	8	41,600,000	21	5	2	1164
M6200	Clinically latent	*M. mulatta*	IV	8	41,600,000	45	306	85	ND
M11800	Clinically latent	*M. mulatta*	IV	8	380	0	0	0	0
M1799§	AIDS	*M. mulatta*	IV	21	780,000	38	14	3	17,764
M5199§	AIDS	*M. mulatta*	IV	24	540,000	38	42	10	23,763
M6199§	AIDS	*M. mulatta*	IV	32	940,000	9	30	5	7181
M5400	AIDS	*M. mulatta*	IV	86	14,000	7	5	2	237
M6700	AIDS	*M. mulatta*	IV	87	19,300	24	17	16	3952
M6900	AIDS	*M. mulatta*	IV	60	355,000	3	2	0	620
M7102	Uninfected	*M. fascicularis*	N/A	N/A	ND	0	0	0	0
M6202	Uninfected	*M. fascicularis*	N/A	N/A	ND	0	0	0	0
M5602	Uninfected	*M. fascicularis*	N/A	N/A	ND	0	0	0	0
M6802	Uninfected	*M. fascicularis*	N/A	N/A	ND	0	0	0	ND
M13402	Uninfected	*M. fascicularis*	N/A	N/A	ND	0	0	0	0

*Real-time RT-PCR was used to determine plasma viral loads; copies of SIV RNA per milliliter of plasma.
†Numbers of RNA-positive cells/mm² determined by ISH.
‡SIV RNA copies/μg total RNA determined by real-time RT-PCR.
§Indicates an animal that has been described previously.[8,15,16,35]
‖Values for samples at 2 weeks after injection were not obtained; values for 1 week after injection are presented.
IT indicates intratracheal; IV, intravenous; N/A, not applicable; ND, not determined.

during AIDS, a larger proportion of SIV-infected cells were localized in follicles, perhaps reflecting the presence of virus trapped on follicular dendritic cells (DCs).[20] Additional correlation analyses revealed a strong positive association between the numbers of SIV vRNA$^+$ cells in HiLN and those previously[15] measured in these animals in spleen ($r = 0.914$, $P < 0.001$), axillary LN ($r = 0.940$, $P < 0.001$), and inguinal LN ($r = 0.82$, $P = 0.004$). Lung tissue SIV burdens, previously measured as SIV vRNA$^+$ cells per 1000 nuclei,[8] also were positively correlated with those in HiLNs ($r = 0.633$, $P = 0.049$).

Simultaneous ISH and IHC staining was performed to identify the cell types productively infected by SIV. We focused on CD68, a marker for monocytes and macrophages, because of its robust staining in fixed tissue sections. Using this approach, we determined that SIV vRNA$^+$ cells in HiLNs were predominantly CD68$^-$ throughout the course of infection (Fig. 1E). The mean percentages of SIV vRNA$^+$ cells that were also CD68$^+$ ranged from 13% to 38% considering all regions of LN and all disease states, except for medullary regions during AIDS (see Fig. 1E), which we note harbored only rare SIV vRNA$^+$ cells. Thus, most SIV vRNA$^+$ cells in HiLNs were CD68$^-$ and presumably T cells.

Array Hybridization Identifies Changes in Expression of Chemokines

To determine the global effects of SIV infection on the immunologic environment in HiLNs, we performed cDNA microarray hybridizations. For this purpose, we fabricated a cDNA microarray to contain 210 unique and immunologically relevant macaque cDNAs.[19] In this series of experiments Cy5-labeled cDNA generated from each HiLN total RNA preparation was cohybridized with Cy3-labeled cDNA generated from a common reference RNA sample composed of pooled uninfected HiLN RNAs. We examined the relative gene expression levels by comparing the group mean values for the normalized expression values (Table 2) and by plotting normalized expression values for individual animals (Fig. 2). Analysis of 20 individual HiLN total RNA preparations revealed only a small subset of mRNAs that were up- or downregulated by 1.5-fold or more (see Table 2) in this complex dynamic tissue. The inflammatory CXC chemokine receptor 3 (CXCR3) ligands CXCL9, CXCL10, and CXCL11 were all consistently among the most upregulated mRNAs early and late after SIV infection. Additional chemokines that were upregulated included the inflammatory chemokines CCL5, CCL2, and CCL8 and the homeostatic chemokines

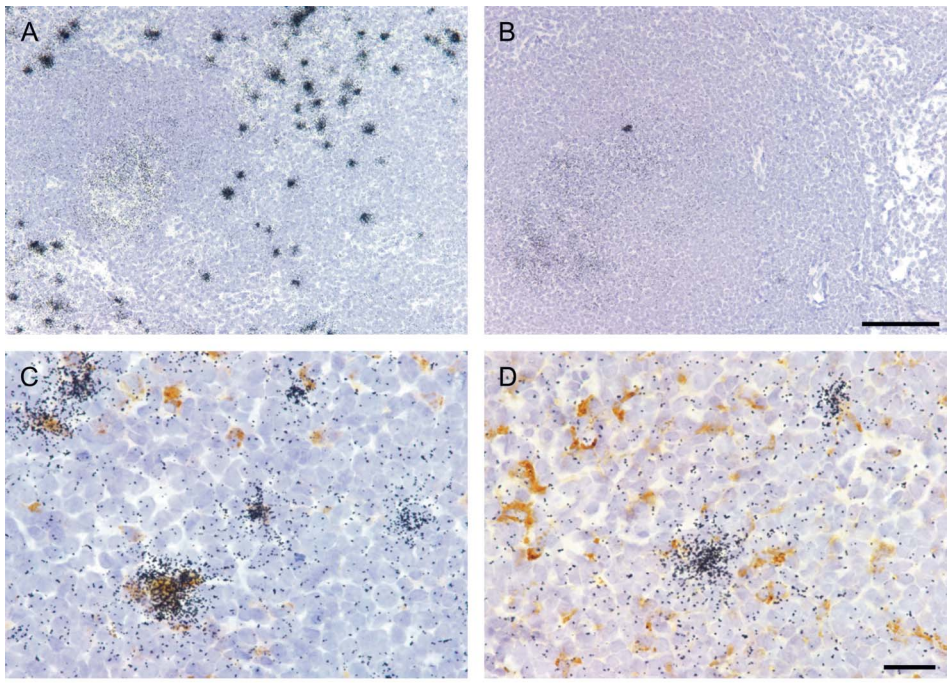

FIGURE 1. ISH analysis of SIV replication in macaque HiLNs. SIV RNA$^+$ cells in HiLN tissue sections were detected using ISH with ^{35}S-labeled riboprobes, with images shown for animals M12000 (A) and M6700 (B). ISH for SIV RNA was combined with immunohistochemistry for the macrophage marker CD68, with images shown for animals M12000 (C) and M6700 (D). The percentages of SIV RNA$^+$ cells that were also CD68$^+$ are summarized in (E) and represented as ⓪ = 0%, ❶ = 1% to 25%, ❷ = 26% to 50%, ❸ = 51% to 75%, and ❹ = 76% to 100%. The size bar in B represents 100 μm (A, B), whereas the bar in D represents 20 μm (C, D). f indicates follicle; m, medulla; pc, paracortex.

TABLE 2. Differentially Expressed MRNAs in Macaque HiLNs Determined by Microarray Hybridization

	Acute IV/UI		Acute IT/UI		Clinical Latency/UI		AIDS/UI	
Gene	Change*	*P*	Change*	*P*	Change*	*P*	Change*	*P*
Upregulated								
CXCL9	3.7	0.022	2.0	0.026	2.7	0.017	3.6	0.003
CXCL10	3.1	0.001	2.8		1.6	0.016	2.0	0.018
CXCL11	2.5	0.004	2.7		1.5		1.7	0.009
SIV LTR	3.5		1.3		1.7		1.6	0.021
CCL5	0.9		0.9		1.0		1.5	
CXCL13	1.6	0.016	1.3		1.0		1.4	0.024
CD16	1.6		1.3		1.1		1.4	
CCL19	1.7	0.014	1.4		1.7		1.3	
Granzyme B	2.2		2.5	0.014	1.1		1.2	
CCL2	1.6		1.5	0.002	1.2		1.2	
Dectin	1.5		1.1		1.0		1.2	
CCL8	1.8	0.041	1.5		1.2		1.1	
Downregulated								
CCL21	−2.6	0.008	−1.8	0.015	−1.6	0.035	−2.8	<0.001
DC-LAMP	−1.7	0.036	−1.7	0.022	−1.4		−2.3	<0.001
CXCL12	−1.6		−1.7	0.043	−1.5		−1.8	0.003
DC-SIGN	−2.4	0.013	−1.4		−1.5		−1.7	0.024
Fascin/p55	−1.4	0.040	−1.4	0.016	−1.2	0.038	−1.6	0.001
CD40L	−1.6	0.008	−1.2		−1.1		−1.5	0.002
LYVE-1	−1.2		−1.3		−1.3		−1.5	0.035
CD28	−1.6	0.013	−1.2		−1.2		−1.4	0.011
LAT	−1.5	0.016	−1.3	0.030	−1.1		−1.3	0.003
TCRβ	−1.5	0.041	−1.3	0.018	−1.2		−1.3	0.008

Criteria for inclusion here are either of the following: group mean ratio >1.5 in any disease state compared with UI or $P < 0.05$ for any. Pairwise comparisons (Mann-Whitney test) of 1 or more disease states relative to UI.

*Ratios of normalized group (disease state) means are shown and have been rank ordered based on the anchor comparison of AIDS/UI.

IT indicates intratracheal; IV, intravenous; UI, uninfected macaques.

CCL19 and CXCL13 (see Table 2). In addition, the cytotoxic granule component granzyme B was upregulated during acute infection. A limited number of the 210 mRNAs examined were downregulated and primarily included the homeostatic chemokines CCL21 and CXCL12; the DC-associated molecules DC-specific lysosome-associated membrane glycoprotein (DC-LAMP), DC-specific ICAM-3 grabbing nonintegrin (DC-SIGN), fascin/p55, and CD40L; and the T-cell–associated molecules CD28, linker of activated T cells (LAT), and T-cell receptor-β (TCRβ).

Real-time RT-PCR was used to measure the expression levels of a subset of these differentially expressed mRNAs

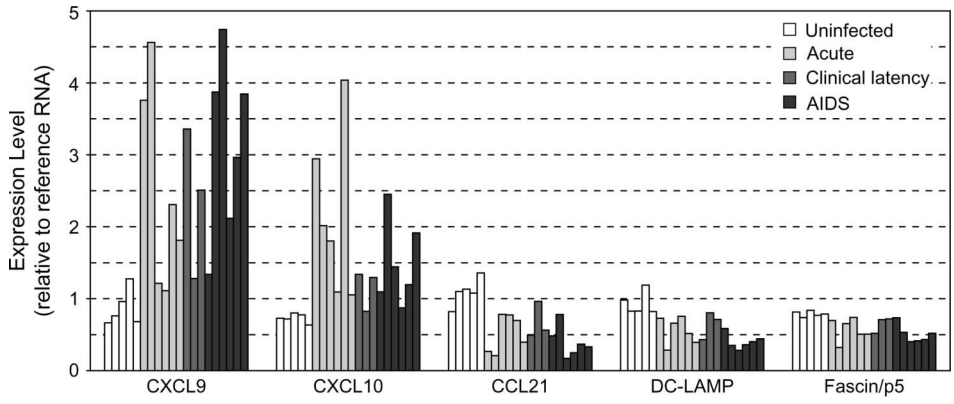

FIGURE 2. DNA array hybridization analyses on HiLN total RNAs from individual rhesus macaques. Using total RNA preparations from individual rhesus macaque HiLNs, cDNA array hybridization was performed as described in the Materials and Methods section. The expression values represent the hybridization signals normalized to multiple endogenous control mRNAs and then to a common reference RNA sample hybridized on each array. Data for individual animals from different disease states are presented for representative genes that increased, decreased, or remained unchanged during SIV infection (mean values are presented in Table 2).

more precisely, focusing mainly on chemokines because of their ability to control the trafficking,[21] survival,[22–24] and cytokine production profiles[25] of immune cells. Using this approach, CXCL9 and CXCL10 mRNAs were confirmed to be significantly increased in expression after SIV infection (Fig. 3), as was mRNA-encoding IFNγ, which is an upstream inducer of these CXCR3 ligands.[26] CCR7 ligands control the homeostatic trafficking of mature DCs and naive T cells into

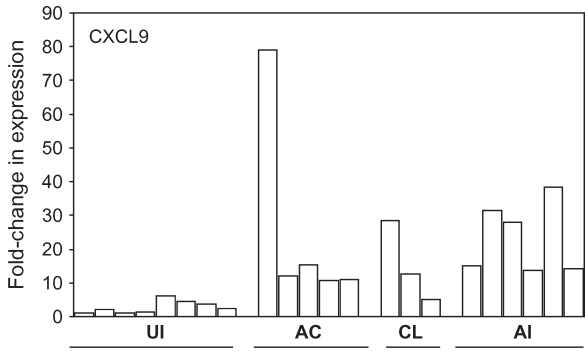

		UI	AC	CL	AI
CXCL9	Mean	2.8	25.7	20.6	23.5
	SEM	0.7	13.3	7.9	4.3
	Ratio (to UI)		**9.2**	**7.4**	**8.4**
	P value		**0.003**	**0.025**	**0.002**
CXCL10	Mean	1.3	17.2	7.8	7.1
	SEM	0.2	6.3	4.9	1.1
	Ratio (to UI)		**13.2**	**6.0**	**5.5**
	P value		**0.003**	**0.014**	**0.002**
IFNγ	Mean	1.6	7.8	3.5	6.6
	SEM	0.2	3.3	0.4	1.1
	Ratio (to UI)		**4.9**	**2.2**	**4.1**
	P value		**0.003**	**0.014**	**0.002**
TLR3	Mean	1.2	3.5	2.7	2.4
	SEM	0.3	1.1	0.7	0.5
	Ratio (to UI)		**2.9**	**2.3**	**2.0**
	P value		**0.019**	0.307	0.053
CCL19	Mean	1.7	3.3	4.3	2.1
	SEM	0.3	0.5	2.3	0.3
	Ratio (to UI)		**1.9**	**2.5**	**1.2**
	P value		**0.013**	0.307	0.302
CCL21	Mean	1.9	0.7	0.7	0.6
	SEM	0.6	0.2	0.3	0.2
	Ratio (to UI)		**0.4**	**0.4**	**0.3**
	P value		0.057	0.683	**0.014**

FIGURE 3. Real-time RT-PCR measurement of mRNA expression in rhesus macaque HiLNs. The comparative C_T method was used to measure the relative mRNA expression levels of key immunologic mRNAs in macaque HiLNs. Data for individual animals are presented in the bar graph for CXCL9 mRNA, with summary data included beneath the graph. Only summary data are presented for the other 5 mRNAs. Statistical comparison between the uninfected (UI) and SIV-infected (AC, acute; CL, clinically latent; AI, AIDS) groups was performed using the Mann-Whitney test. *P* values <0.05 are noted in bold.

LNs,[21] and we found that expression of CCL19 mRNA was significantly upregulated in HiLNs during the acute phase of infection only, whereas CCL21 mRNA was decreased during AIDS (see Fig. 3). Finally, TLR3 mRNA was also increased during acute infection, as has been shown for axillary LNs.[16] Overall, these findings were concordant with the array hybridization data.

Correlation analyses were performed to identify possible associations between the expression levels of these mRNAs and revealed that CXCL9, CXCL10, and CCL19 mRNA levels were all positively correlated with each other ($r = 0.54$ to 0.55, $P < 0.01$ for all 3 pairwise comparisons) and with tissue-associated SIV levels ($P = 0.033$ to 0.019) but not with plasma viral loads. CCL21 mRNA levels were negatively correlated with tissue-associated SIV RNA levels ($P = 0.020$). The mRNA levels for IFNγ correlated with CXCL9 ($P < 0.001$), CXCL10 ($P = 0.007$), and tissue-associated SIV ($P = 0.029$) RNA levels, and marginally so with CCL19 ($P = 0.054$) RNA levels. Finally, TLR3 mRNA levels were positively correlated with tissue-associated SIV levels ($P = 0.022$). These data indicate that levels of local viral replication were correlated with increased expression of proinflammatory chemokine mRNAs during SIV infection and decreased expression of a homeostatic chemokine.

Localization of CXCL9 and CCL19 mRNAs to Paracortical Areas in HiLNs

Using ISH, we found that CXCL9 and CCL19 mRNAs were expressed nearly exclusively in the T-cell– and DC-rich paracortical region of HiLNs, with only minimal expression in follicles (Fig. 4). CXCL9 levels in paracortex were increased throughout all stages of SIV infection as compared with uninfected macaques. CCL19 was similarly expressed in HiLN paracortical regions; expression levels increased during acute infection and clinical latency and then decreased slightly during AIDS. Both chemokines showed only limited increases in expression in follicular and medullary regions of HiLNs throughout the course of SIV infection.

ISH detection of chemokine mRNAs was next coupled with IHC staining for CD68 (monocytes/macrophages) or fascin/p55 (DCs) to identify the sources of chemokine production. The proportion of CXCL9 signal estimated to be attributed to $CD68^+$ macrophages or $fascin/p55^+$ DCs ranged for both cell types from approximately 25% to 50% regardless of an animal's SIV infection status (see Fig. 4). The findings for CCL19 $mRNA^+$ cells were similar to those for CXCL9 (see Fig. 4). These data indicate that macrophages and DCs comprise a large proportion of the cells that express the increased CXCL9 and CCL19 mRNAs during SIV infection.

Increased Cellular Proliferation in HiLNs After SIV Infection

We next performed immunostaining and quantitative image analyses for Ki67 to determine the overall proliferative state of the local environment. There were increases in the percentages of $Ki67^+$ cells in all regions of HiLNs throughout the entire course of infection (Fig. 5). Two-color immunofluorescence staining for Ki67 and CD3, CD20, CD68,

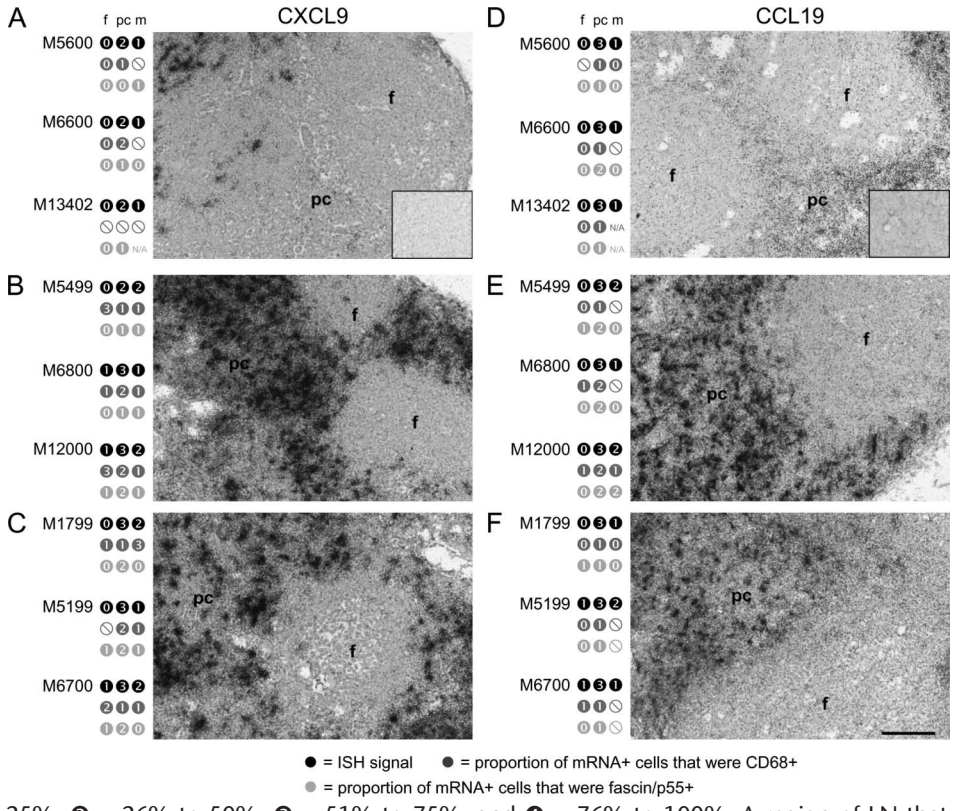

FIGURE 4. ISH localization of CXCL9 and CCL19 mRNAs in rhesus macaque HiLNs. HiLN tissue sections were hybridized in situ with CXCL9- and CCL19-specific ^{35}S-labeled riboprobes, and representative images are presented of paracortical and follicular regions from uninfected (A, D), acutely infected (B, E), and AIDS-developing (C, F) macaques. The insets in A and D represent parallel hybridization with the sense control riboprobes. Histologic scores were assigned to each tissue section based on the ISH signal, which is represented by numeric values in the black circles: ⓿ = −, ❶ = +, ❷ = ++, and ❸ = +++. ISH for CXCL9 or CCL19 mRNAs was performed simultaneously with IHC for CD68 or p55/fascin. Tissue sections were closely examined, and histologic scores were assigned to represent estimates of percentages of RNA signals attributable to cells expressing the cell type–specific antigens for the indicated macaques, with dark gray circles representing the percentages for CD68$^+$ cells and light gray circles representing the percentages for p55/fascin$^+$ cells: ⓿ = 0%, ❶ = 1% to 25%, ❷ = 26% to 50%, ❸ = 51% to 75%, and ❹ = 76% to 100%. A region of LN that was present in the section but did not have any ISH signal is represented by ⦸. N/A denotes that a tissue section did not contain appreciable area from that region of LN. The size bar in F represents 100 μm (A–F). f indicates follicle; m, medulla; pc, paracortex.

fascin/p55, or CXCR3 revealed that in the absence of infection, few of the Ki67$^+$ cells were CD20$^+$ or CD68$^+$, and approximately half of them could be costained for CD3$^+$, CXCR3$^+$, or fascin/p55$^+$, all of which are likely to be overlapping subsets. Although the numbers of Ki67$^+$ cells increased during the course of infection, the relative proportions staining with individual cell type markers did not change appreciably, except for CD20, the proportion of which increased by 1.6-fold during AIDS. Therefore, there was an early and sustained increase in the extent of local cellular proliferation consistent with the inflammatory environment created by increased expression of inflammatory chemokines.

To determine whether the Ki67$^+$ cells were a major target for productive SIV infection, we combined detection of SIV mRNA and Ki67 antigen in HiLN tissue sections (eg, Fig. 6) from a subset of acute-stage and AIDS-positive animals. A total of 1068 SIV mRNA$^+$ cells were viewed and scored, and 21% were found to be Ki67$^+$. In HiLNs from the animals with AIDS, 32% of SIV-positive cells were Ki67$^+$, whereas in HiLNs from acutely infected animals, only 15% of SIV-positive cells were Ki67$^+$. In all animals, the medullary microanatomic compartment of HiLNs harbored a subset of SIV-positive cells, with greatest proportion being Ki67$^+$ (48% during AIDS and 18% during acute infection). These HiLN data are consistent with previous findings that proliferating cells are excellent substrates for viral replication but that cells do not need to be discernibly dividing to serve as targets for viral replication.[27]

DISCUSSION

In this study, we have examined comprehensively HiLNs from uninfected macaques and from macaques in different stages of SIV infection and disease to determine the effects of infection on the local immunologic environment in lung-draining LNs. Using array hybridization, real-time RT-PCR, and histologic analyses, we found that there is an inflammatory response that occurs after SIV infection, which is composed of an IFNγ/CXCR3 ligand (ie, type 1) axis and is associated with increased local cellular activation and appreciable levels of local SIV replication, all of which could contribute to overall loss of immune function.

With respect to the virologic events in lung-draining LNs, we found that the levels of local SIV replication correlated with the levels of virus in plasma and the levels in other secondary lymphoid tissues. These findings indicate that lung-draining LNs are not unique with respect to their ability to support or suppress viral replication. The targets for infection throughout the course of disease remained predominantly CD68$^-$, and therefore not macrophages, consistent with other lymphoid tissues in SIV-infected macaques[8] and HIV-1–infected humans.[28] This is interesting, given that the targets for infection in the respective lung tissues switch from

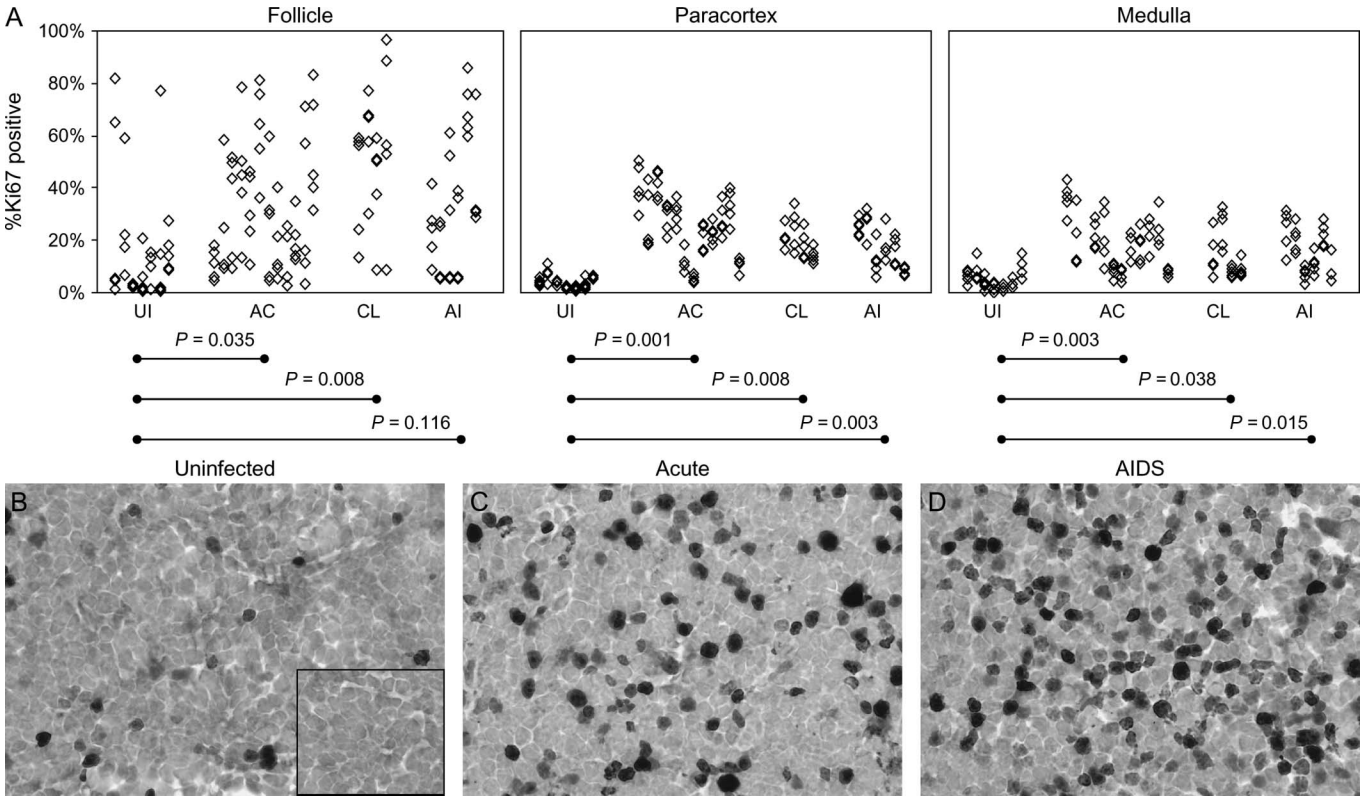

FIGURE 5. Increased cellular proliferation in macaque HiLNs during SIV infection. HiLN tissue sections were stained for Ki67, and quantitative image capture and analysis was used to determine the percentages of Ki67$^+$ cells in follicular, paracortical, and medullary regions of LN. A, Individual data points in representative random images obtained from individual ×600 microscopic fields. AC indicates acutely infected; AI, AIDS; CL, clinically latent; UI, uninfected. B–D, Images of representative tissue section are all of paracortical regions of LN. The inset in B represents a subjacent tissue section stained in parallel with an isotype control antibody. The differences between the UI and AC or AI groups were compared using the Mann-Whitney test.

CD68$^-$ to CD68$^+$ as disease progresses.[8] Therefore, despite the drainage of free virus and/or cell-associated virus from lung tissues through the lymphatics, there is an unidentified restriction on the target cell populations that are productively infected by SIV in the lung-draining LNs.

Array hybridizations revealed that inflammatory chemokines were among the most upregulated genes after infection and that a chemokine that controls DC migration (CCL21) and a subset of DC-associated genes were among the most downregulated genes. Given the central role of chemokines in regulating the trafficking of cells to LNs from blood and lymphatics,[21] we focused much of our attention on them.

The inflammatory environment we identified in lung-draining LNs consisted of increased levels of IFNγ and IFNγ-inducible CXCR3 ligands, CXCL9, CXC40, and CXCL11, and increased proportions of proliferating cells. During AIDS, these 3 chemokines, along with follicle-associated CXCL13, comprised the only statistically significant increases in mRNA expression observed by array hybridization among the 210 targets examined. Given that a limitation of our study was the dilution effect associated with measuring mRNA expression levels from homogenized tissues, these significant differences are that much more striking. This increase in inflammatory chemokines in lung-draining LNs is consistent with what we[15] and others[29] have found in LNs draining nonpulmonary tissues, such as axillary LN and spleen. The model we originally proposed,[15] in which a type 1 positive feedback loop is operating in peripheral LN and spleen after SIV infection and that is composed of ongoing IFNγ induction of CXCR3 ligands and subsequent recruitment of additional IFNγ-producing cells, is supported by our findings here and extended to include mucosal draining LNs. One outcome of these events is decreased availability of CXCR3$^+$ effector T cells in blood for migration to the lungs because of ectopic recruitment to HiLNs and other LNs.

During the course of SIV infection, there was a dramatic increase in the frequency of Ki67$^+$ cells in HiLNs, indicating that they were undergoing or had recently undergone cell division. Increased levels of cellular proliferation have been identified in other macaque lymphoid tissues during SIV infection.[27,30,31] It is not yet known whether these cells were proliferating when they entered the HiLNs or were stimulated to proliferate after arriving there. Our observation that a large proportion of the Ki67$^+$ cells were also CXCR3$^+$, however, suggests that recruitment by the increased CXCR3 ligands contributes to increased levels of proliferating cells. In addition, CXCL9 can stimulate T-cell proliferation,[32] and

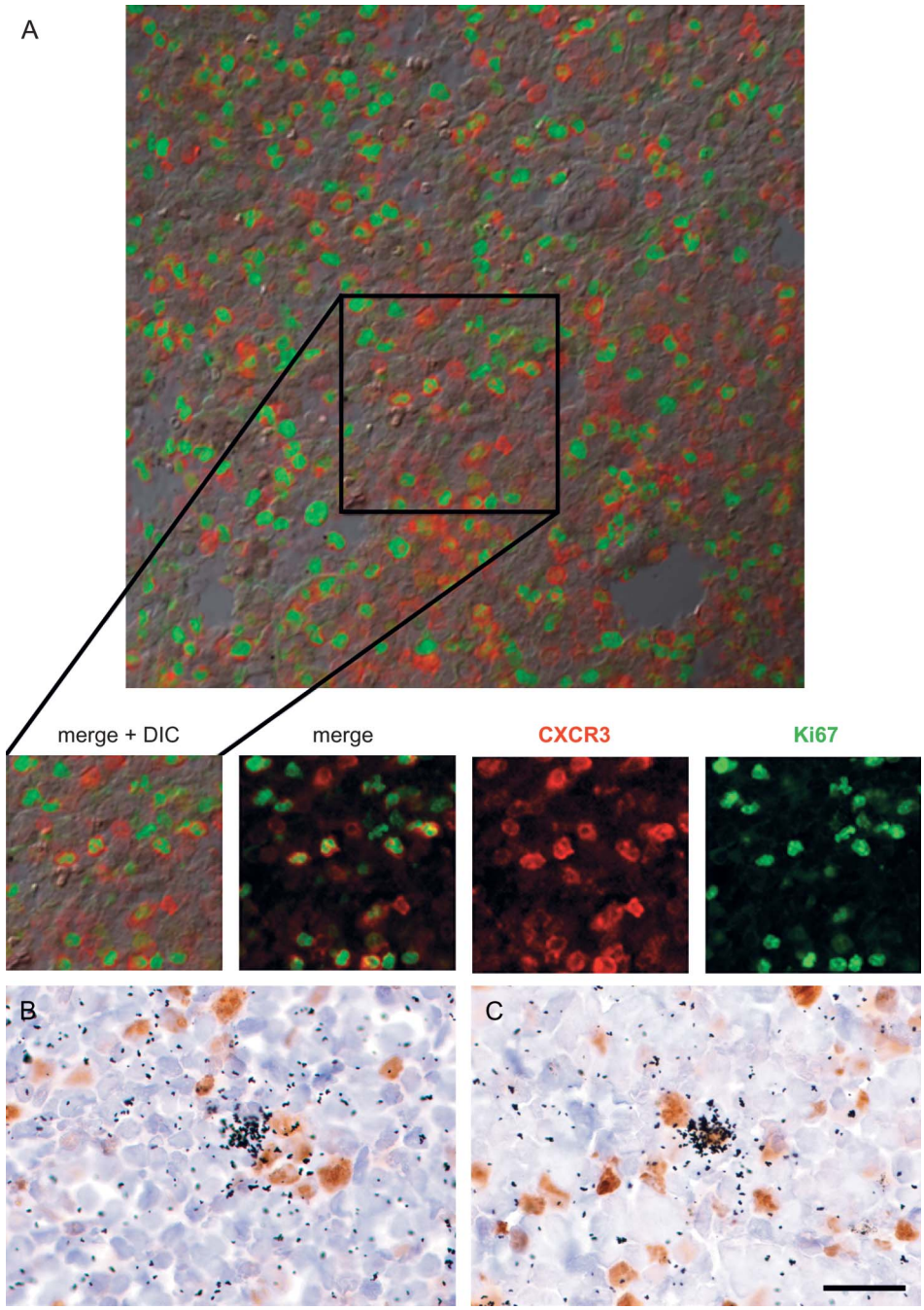

FIGURE 6. Simultaneous detection of Ki67/CXCR3 and Ki67/SIV RNA in rhesus macaque HiLN tissue sections. A, Simultaneous immunostaining for Ki67 (AlexaFluor 488; green) and CXCR3 (AlexaFluor 647; red) was performed in macaque HiLN tissue sections and examined using laser scanning confocal microscopy. Immunostaining for Ki67 was combined with ISH for SIV RNA, and representative images are shown for an SIV-positive/Ki67$^-$ cell (B) and for an SIV-positive/Ki67$^+$ cell (C). The size bar in C represents 20 μm (B, C). The animals represented by these images are M6800 (A), M6700 (B), and M1799 (C).

the increased CXCL9, CXCL10, and CXCL11 expression could contribute directly to increased local cellular proliferation. The significance of increased local proliferation relates to the increased susceptibility of these cells to viral infection and their propensity to produce large amounts of virus[27,30] and to the potential for these cells to be activated and undergo activation-induced cell death.[33] Increased apoptosis could contribute to the local inflammatory response through stimulation of TLR3 by means of double-stranded RNA (dsRNA) associated with apoptotic bodies.[34] Notably, TLR3 is upregulated in peripheral LNs[16] and HiLNs (see Fig. 3) and is available to contribute to increased expression of CXCR3 ligands.

In addition to the induction of inflammatory CXCR3 ligands, we observed a dichotomous effect of SIV infection on expression of the CCR7 ligands CCL21 and CCL19, which control the migration of mature DCs, naive T cells, and central memory T cells to secondary lymphoid tissues.[21] We found that CCL21 was abundant in the absence of SIV infection and then decreased throughout the course of infection, whereas CCL19 was minimally expressed before infection and increased during acute infection before declining slightly during

AIDS. These findings are consistent with our previous findings[35] as well as with those of others[29] in other lymphoid compartments, including axillary LN and spleen. It is not clear whether overall recruitment of $CCR7^+$ cells is the result of the net local effects of CCL21 and CCL19 combined or whether there are chemokine-specific effects. CCL21 and CCL19 provide a survival signal to DCs through the activation of the Akt1 kinase.[24] They also interact with and signal differentially through CCR7[23] and have different effects on ectopic lymphoid tissue generation in CCL19 or CCL21 knockout mice.[36] Increased expression of CCL19 after SIV infection could contribute to the type 1 polarized environment and local proliferation, because it can induce T cell proliferation in DC/T cell cocultures and can skew stimulated T cells toward a type 1 phenotype,[37] which has also been observed with CXCL10.[25] Interestingly, CCL19 and CCL21 contribute to activation-induced cell death in mice, and alterations to the combined local levels of these CCR7 ligands could have complex consequences on the recruitment and survival of DCs and the recruitment, proliferation, loss, and polarization of T cells, all of which has an impact on overall immune function.

In summary, we have shown that pathogenic SIV infection leads to the induction of a type 1 inflammatory response in lung-draining LNs involving the CXCR3 ligands CXCL9, CXCL10, and CXCL11 and the CCR7 ligand CCL19. These inflammatory mediators likely increase the recruitment of activated T cells, the proliferation of T cells, and the recruitment of DCs and naive T cells. These findings suggest that testing therapeutics inhibiting these chemokines or chemokine receptors in a preclinical model such as the SIV/macaque system can provide insight into whether such anti-inflammatory approaches may have clinical benefit for HIV-1–infected individuals.

ACKNOWLEDGMENTS

The authors thank Nicole Banichar, Shawn Begnston, Dr. Saverio Capuano III, Holly Casamassa, Stephanie Casino, Dawn McClemens-McBride, Dr. Dave Meleason, Melanie Osborn O'Malley, Shane Ritchea, and Dr. Anita Trichel for excellent assistance with project coordination and animal care; Dr. Craig Fuller for helpful discussion regarding the early statistical analyses; Dr. Simon Barratt-Boyes for access to 3 uninfected rhesus macaque LNs; Dr. Edward Klein for assistance in initial histopathologic evaluations; Dr. Carey Balaban for advice and assistance with transcardial perfusion; Jason Devlin for advice and assistance in the use of the confocal microscope; Veronica Pedregon for assistance with statistical analyses; and Dr. Shulin Qin and Kristi Gaus for advice and helpful discussions.

REFERENCES

1. Jellinger KA, Setinek U, Drlicek M, et al. Neuropathology and general autopsy findings in AIDS during the last 15 years. *Acta Neuropathol (Berl)*. 2000;100:213–220.
2. Masliah E, DeTeresa RM, Mallory ME, et al. Changes in pathological findings at autopsy in AIDS cases for the last 15 years. *AIDS*. 2000;14:69–74.
3. Boyton RJ. Infectious lung complications in patients with HIV/AIDS. *Curr Opin Pulm Med*. 2005;11:203–207.
4. Collins KR, Quinones-Mateu ME, Toossi Z, et al. Impact of tuberculosis on HIV-1 replication, diversity, and disease progression. *AIDS Rev.* 2002; 4:165–176.
5. Board KF, Patil S, Lebedeva I, et al. Experimental Pneumocystis carinii pneumonia in simian immunodeficiency virus-infected rhesus macaques. *J Infect Dis*. 2003;187:576–588.
6. Beck JM, Rosen MJ, Peavy HH. Pulmonary complications of HIV infection. Report of the Fourth NHLBI Workshop. *Am J Respir Crit Care Med*. 2001;164:2120–2126.
7. Mankowski JL, Carter DL, Spelman JP, et al. Pathogenesis of simian immunodeficiency virus pneumonia: an immunopathological response to virus. *Am J Pathol*. 1998;153:1123–1130.
8. Fuller CL, Choi YK, Fallert BA, et al. Restricted SIV replication in rhesus macaque lung tissues during the acute phase of infection. *Am J Pathol*. 2002;161:969–978.
9. Embretson J, Zupancic M, Ribas JL, et al. Massive covert infection of helper T-lymphocytes and macrophages by HIV during the incubation period of AIDS. *Nature*. 1993;362:359–362.
10. Pantaleo G, Graziosi C, Demarest JF, et al. HIV-infection is active and progressive in lymphoid-tissue during the clinically latent stage of disease. *Nature*. 1993;362:355–358.
11. Reinhart TA, Rogan MJ, Huddleston D, et al. Simian immunodeficiency virus burden in tissues and cellular compartments during clinical latency and AIDS. *J Infect Dis*. 1997;176:1198–1208.
12. Chakrabarti L, Cumont MC, Montagnier L, et al. Variable course of primary simian immunodeficiency virus infection in lymph nodes: relation to disease progression. *J Virol*. 1994;68:6634–6643.
13. Murphey-Corb M, Martin LN, Rangan SR, et al. Isolation of an HTLV-III-related retrovirus from macaques with simian AIDS and its possible origin in asymptomatic mangabeys. *Nature*. 1986;321:435–437.
14. Fallert BA, Reinhart TA. Improved detection of simian immunodeficiency virus RNA by in situ hybridization in fixed tissue sections: combined effects of temperatures for tissue fixation and probe hybridization. *J Virol Methods*. 2002;99:23–32.
15. Reinhart TA, Fallert BA, Pfeifer ME, et al. Increased expression of the inflammatory chemokine CXC chemokine ligand 9/monokine induced by interferon-gamma in lymphoid tissues of rhesus macaques during simian immunodeficiency virus infection and acquired immunodeficiency syndrome. *Blood*. 2002;99:3119–3128.
16. Sanghavi SK, Reinhart TA. Increased expression of TLR3 in lymph nodes during simian immunodeficiency virus infection: implications for inflammation and immunodeficiency. *J Immunol*. 2005;175:5314–5323.
17. Godfrey TE, Kim SH, Chavira M, et al. Quantitative mRNA expression analysis from formalin-fixed, paraffin-embedded tissues using 5′ nuclease quantitative reverse transcription-polymerase chain reaction. *J Mol Diagn*. 2000;2:84–91.
18. Fuller DH, Rajakumar PA, Wilson LA, et al. Induction of mucosal protection against primary, heterologous simian immunodeficiency virus by a DNA vaccine. *J Virol*. 2002;76:3309–3317.
19. Schaefer TM, Fuller CL, Basu S, et al. Increased expression of interferon-inducible genes in macaque lung tissues during simian immunodeficiency virus infection. *Microbes Infect*. 2006;8:1839–1850.
20. Reinhart TA, Rogan MJ, Viglianti GA, et al. A new approach to investigating the relationship between productive infection and cytopathicity in vivo. *Nat Med*. 1997;3:218–221.
21. Cyster JG. Chemokines and cell migration in secondary lymphoid organs. *Science*. 1999;286:2098–2102.
22. Kim JW, Ferris RL, Whiteside TL. Chemokine C receptor 7 expression and protection of circulating CD8+ T lymphocytes from apoptosis. *Clin Cancer Res*. 2005;11:7901–7910.
23. Kohout TA, Nicholas SL, Perry SJ, et al. Differential desensitization, receptor phosphorylation, beta-arrestin recruitment, and ERK1/2 activation by the two endogenous ligands for the CC chemokine receptor 7. *J Biol Chem*. 2004;279:23214–23222.
24. Sanchez-Sanchez N, Riol-Blanco L, de la Rosa G, et al. Chemokine receptor CCR7 induces intracellular signaling that inhibits apoptosis of mature dendritic cells. *Blood*. 2004;104:619–625.
25. Gangur V, Simons FE, HayGlass KT. Human IP-10 selectively promotes dominance of polyclonally activated and environmental antigen-driven IFN-gamma over IL-4 responses. *FASEB J.* 1998;12: 705–713.

26. Farber JM. HuMig: a new human member of the chemokine family of cytokines. *Biochem Biophys Res Commun*. 1993;192:223–230.
27. Zhang Z, Schuler T, Zupancic M, et al. Sexual transmission and propagation of SIV and HIV in resting and activated CD4+ T cells. *Science*. 1999;286:1353–1357.
28. Schacker T, Little S, Connick E, et al. Productive infection of T cells in lymphoid tissues during primary and early human immunodeficiency virus infection. *J Infect Dis*. 2001;183:555–562.
29. Clay CC, Rodrigues DS, Harvey DJ, et al. Distinct chemokine triggers and in vivo migratory paths of fluorescein dye-labeled T lymphocytes in acutely simian immunodeficiency virus SIVmac251-infected and uninfected macaques. *J Virol*. 2005;79:13759–13768.
30. Zhang ZQ, Wietgrefe SW, Li Q, et al. Roles of substrate availability and infection of resting and activated CD4+ T cells in transmission and acute simian immunodeficiency virus infection. *Proc Natl Acad Sci USA*. 2004;101:5640–5645.
31. Li Q, Duan L, Estes JD, et al. Peak SIV replication in resting memory CD4+ T cells depletes gut lamina propria CD4+ T cells. *Nature*. 2005; 434:1148–1152.
32. Whiting D, Hsieh G, Yun JJ, et al. Chemokine monokine induced by IFN-gamma/CXC chemokine ligand 9 stimulates T lymphocyte proliferation and effector cytokine production. *J Immunol*. 2004;172:7417–7424.
33. Green DR, Droin N, Pinkoski M. Activation-induced cell death in T cells. *Immunol Rev.* 2003;193:70–81.
34. Kariko K, Ni HP, Capodici J, et al. mRNA is an endogenous ligand for Toll-like receptor 3. *J Biol Chem*. 2004;279:12542–12550.
35. Choi YK, Fallert BA, Murphey-Corb MA, et al. Simian immunodeficiency virus dramatically alters expression of homeostatic chemokines and dendritic cell markers during infection in vivo. *Blood*. 2003;101: 1684–1691.
36. Luther SA, Bidgol A, Hargreaves DC, et al. Differing activities of homeostatic chemokines CCL19, CCL21, and CXCL12 in lymphocyte and dendritic cell recruitment and lymphoid neogenesis. *J Immunol*. 2002; 169:424–433.
37. Marsland BJ, Battig P, Bauer M, et al. CCL19 and CCL21 induce a potent proinflammatory differentiation program in licensed dendritic cells. *Immunity.* 2005;22:493–505.

